UNIVERSITY OF WEST BOHEMIA

Applied and Computational Mechanics 3 (2009) 101–110

Applied and Computational Mechanics

Smoothed particle hydrodynamics modelling in continuum mechanics: fluid-structure interaction

L. Lobovský[a,*], P. H. L. Groenenboom[b]

[a] *Department of Mechanics, Faculty of Applied Sciences, University of West Bohemia, Univerzitní 22, 306 14 Plzeň, Czech Republic*
[b] *ESI Group Netherlands, Rotterdamseweg 183 C, 2629 HD Delft, Netherlands*

Received 8 September 2008 ; received in revised form 18 April 2009

Abstract

Within this study, the implementation of the smoothed particle hydrodynamics (SPH) method solving the complex problem of interaction between a quasi-incompressible fluid involving a free surface and an elastic structure is outlined. A brief description of the SPH model for both the quasi-incompressible fluid and the isotropic elastic solid is presented. The interaction between the fluid and the elastic structure is realised through the contact algorithm. The results of numerical computations are confronted with the experimental as well as computational data published in the literature.

© 2009 University of West Bohemia. All rights reserved.

Keywords: smoothed particle hydrodynamics, meshless methods, fluid dynamics, elastodynamics, fluid-structure interaction

1. Introduction

The computational solution of the fluid-structure interaction (FSI) is a complex problem which is a topical issue in numerous engineering applications, from the mechanical and civil engineering through the environmental engineering to biomechanics and biomedical engineering. Within this study a special attention is paid to the interaction between a quasi-incompressible fluid (liquid) and an isotropic elastic solid. The FSI problem is decomposed to synchronous solution of the fluid dynamics and the elastodynamics, while the interaction algorithm is applied at the fluid-solid interface. The mechanical response of the fluid and of the solid is solved separately using the smoothed particle hydrodynamics (SPH) method and the particle-to-particle contact algorithm is applied in order to solve their interaction.

The SPH method is a truly meshless Lagrangian numerical technique introduced to solve gas dynamics problems in astrophysics in late 1970s, [5] and [11]. Since then, the flexibility of its meshless Lagrangian nature and ease of implementation is well employed within numerous branches of computational physics, see e.g. [10, 20]. Its meshless character makes the method very flexible and enables simulations of physical problems which might be difficult to capture by conventional grid-based methods. As this contribution is concerned about its application within computational continuum mechanics, it should be emphasised that the SPH method could be advantageous e.g. during simulations of materials undergoing large deformations, brittle solids, free surface flows or fluid-structure interaction.

Besides a number of publications on numerical modelling of fluid to structure or structure to structure interaction by coupling the SPH method to mesh-based methods, e.g. [4, 7, 8, 21],

*Corresponding author. Tel.: +420 377 632 336, e-mail: lobo@kme.zcu.cz.

there are several studies related to computational analysis of these problems purely by the SPH approach, e.g. [1, 2] or [17]. Within this study, a purely SPH based solution of the FSI problem is utilised. Standard SPH models for laminar flow of a quasi-incompressible fluid, e.g. [12, 3] or [10], and for an isotropic elastic material, e.g. [9] or [6], are adopted and implemented within a special SPH code.

Antoci et al., [1], presented a complex FSI algorithm utilising an approximate SPH evaluation of a surface integral. That requires an identification of the contact surface which might be challenging especially when fractures are involved. Herewith, a simplified interaction algorithm, which enables solution of an interaction between fluid and solid without a need to define the contact surface, is implemented. The FSI is realised by application of contact forces acting between the particles at the contact interface. This approach was previously used by Campbell et al., [2], for a solution of the contact between elastic bodies.

The stability of the performance of the SPH code is enforced by an application of additional numerical stabilising terms (artificial viscosity, artifical stress and correction of particle motion). The rigid boundary conditions are represented by two sets of boundary particles while an additional corrective term may be applied.

The implemented SPH code is applied to a test problem which was originally performed and published by Antoci et al., [1], whose experimental as well as computational results are used for validation of the presented code.

2. SPH model

Within the SPH formulation, the computational domain is discretised by a finite set of interpolating points (particles) with invariant coordinates in the material frame. The SPH particles represent a finite mass of the discretised continuum and carry the information about all physical variables which are evaluated at their positions. The function values and their derivatives at a specific particle are interpolated from the function values at surrounding particles using the interpolating (smoothing) function and its derivatives, respectively,

$$f_i = \sum_j \frac{m_j}{\rho_j} f_j W(|\mathbf{r}_i - \mathbf{r}_j|, h), \tag{1}$$

$$\nabla_i f_i = \sum_j \frac{m_j}{\rho_j} f_j \nabla_i W(|\mathbf{r}_i - \mathbf{r}_j|, h), \tag{2}$$

where m is the mass, ρ is the density and W is the interpolating (smoothing) function with a continuous derivative $\nabla_i W$. The index i, j respectively, denotes the variables at the particle i, j respectively, and ∇_i denotes a derivative according to $\mathbf{r}_i$ which is the position vector.

The smoothing function W is defined so that its value monotonously decreases as the distance between particles increases. It has a compact support domain, which radius is defined by the smoothing length h. The smoothing function is normalised and in the limit case, when the smoothing length goes to zero, the smoothing function becomes the Dirac delta function, see e.g. [10] for details on deriving the general SPH equations and the smoothing functions. Within this study, the cubic B-spline smoothing function is applied, [12].

2.1. Quasi-incompressible fluid

The conservation laws describing the fluid dynamics are discretised using the relations (1) and (2) so that a symetric form of the SPH governing equations satisfying the third Newton's law is

obtained. The conservation of mass is assured by the continuity equation

$$\frac{\mathrm{d}\rho_i}{\mathrm{d}t} = \sum_j m_j(\mathbf{v}_i - \mathbf{v}_j) \cdot \nabla_i W_{ij}, \tag{3}$$

where $\mathbf{v}$ is the velocity vector and $W_{ij} = W(|\mathbf{r}_i - \mathbf{r}_j|, h)$.

The fluid motion is governed by SPH approximation of the Navier-Stokes equation

$$\frac{\mathrm{d}\mathbf{v}_i}{\mathrm{d}t} = \mathcal{P}_i + \mathcal{V}_i + \mathbf{f}_i, \tag{4}$$

where $\mathcal{P}_i$ is the pressure term, $\mathcal{V}_i$ represents the viscous forces and $\mathbf{f}_i$ is the body force. The pressure term is derived so that

$$\mathcal{P}_i = -\sum_j m_j \left(\frac{p_i}{\rho_i^2} + \frac{p_j}{\rho_j^2} \right) \nabla_i W_{ij}, \tag{5}$$

where p is the pressure. The viscous forces are modelled by a term derived by Morris et al. [16]

$$\mathcal{V}_i = \sum_j 2\mu \frac{m_j}{\rho_i \rho_j} \frac{(\mathbf{r}_i - \mathbf{r}_j) \cdot \nabla_i W_{ij}}{|\mathbf{r}_i - \mathbf{r}_j|^2 + \eta^2} (\mathbf{v}_i - \mathbf{v}_j), \tag{6}$$

which implies a representation of the second derivative by a combination of a standard SPH and a finite difference approximation of the first derivative. The symbol μ stands for the dynamic viscosity of the fluid and $\eta^2 = 0.01h^2$ is a corrective constant avoiding a creation of singularity when particles are approaching each other.

The presented SPH model implies the quasi-incompressible representation of the fluid through the equation of state, [12],

$$p_i = {}^0p + K \left[\left(\frac{\rho_i}{{}^0\rho} \right)^{\Gamma} - 1 \right], \tag{7}$$

where K is the bulk modulus

$$K = {}^0\rho \frac{{}^0c^2}{\Gamma}. \tag{8}$$

Constants ${}^0p$ and ${}^0\rho$ indicate the initial pressure and the initial density respectively. The initial sound speed value ${}^0c$ is a numerical parameter which is estimated so that the resulting Mach number of the modelled flow is less than 0.1. A constant parameter Γ is usually set equal to 7.

2.2. Elastic solid

Within the SPH model of elastic solid material, the conservation of mass is represented by the continuity equation (3) as it is done within the model of fluid. The conservation of momentum for the elastic material is derived analogously to the equation of motion (4). The resulting SPH equation of motion utilising the Einstein's summation convention according to the coordinates α and β may be written as follows

$$\frac{\mathrm{d}v_i^\alpha}{\mathrm{d}t} = \sum_j m_j \left(\frac{\sigma_i^{\alpha\beta}}{\rho_i^2} + \frac{\sigma_j^{\alpha\beta}}{\rho_j^2} \right) \frac{\partial W_{ij}}{\partial x_i^\beta} + f^\alpha. \tag{9}$$

The stress tensor σ is defined so that

$$\sigma_i^{\alpha\beta} = -p_i\delta^{\alpha\beta} + S_i^{\alpha\beta}, \tag{10}$$

where p is the hydrostatic pressure, $S^{\alpha\beta}$ is the deviatoric stress and $\delta^{\alpha\beta}$ is the Kronecker delta. The rate of change of the deviatoric stress is given according to the Jaumann's formulation of the Hooke's law

$$\frac{\mathrm{d}S_i^{\alpha\beta}}{\mathrm{d}t} = 2G\left(\dot{\epsilon}_i^{\alpha\beta} - \frac{1}{3}\delta^{\alpha\beta}\dot{\epsilon}_i^{\gamma\gamma}\right) + S_i^{\alpha\gamma}\Omega_i^{\beta\gamma} + \Omega_i^{\alpha\gamma}S_i^{\gamma\beta}, \tag{11}$$

where G is the shear modulus of the modelled material, $\dot{\epsilon}$ and Ω are the strain rate and rotation rate tensors respectively. The hydrostatic pressure p is calculated from the state equation

$$p_i = {}^0c^2(\rho_i - {}^0\rho), \tag{12}$$

while the bulk modulus of the represented material is given so that

$$K = {}^0\rho\,{}^0c^2. \tag{13}$$

3. Stabilising terms

The SPH governing equations may be extended by additional artificial numerical terms which helps to keep the numerical simulation stable. Then, the pressure term in the Navier-Stokes equation (4) becomes

$$\mathcal{P}_i = -\sum_j m_j\left(\frac{p_i}{\rho_i^2} + \frac{p_j}{\rho_j^2} + \Pi_{ij} + R_{ij}\phi_{ij}^n\right)\nabla_i W_{ij} \tag{14}$$

and the equation of motion for the elastic solid (9) becomes

$$\begin{aligned}\frac{\mathrm{d}v_i^\alpha}{\mathrm{d}t} &= \sum_j m_j\left(\frac{\sigma_i^{\alpha\beta}}{\rho_i^2} + \frac{\sigma_j^{\alpha\beta}}{\rho_j^2}\right)\frac{\partial W_{ij}}{\partial x_i^\beta} + \\ &\quad + \sum_j m_j\left(\Pi_{ij}\delta^{\alpha\beta} + R_{ij}^{\alpha\beta}\phi_{ij}^n\right)\frac{\partial W_{ij}}{\partial x_i^\beta} + f^\alpha.\end{aligned} \tag{15}$$

The artificial viscosity term $\Pi_{ij}\delta^{\alpha\beta}$ is applied in order to smooth the unphysical numerical oscillations, [15], while the artificial stress term $R_{ij}^{\alpha\beta}\phi_{ij}^n$ (note that n is the exponent) reduces the tensile instability, [14]. The exact meaning of terms Π_{ij}, $R_{ij}^{\alpha\beta}$ and ϕ_{ij} is explained in section 3.1 and 3.2, $\delta^{\alpha\beta}$ is the Kronecker delta.

3.1. Artificial viscosity

The artificial viscosity is defined as a combination of terms analogous to bulk and von Neumann-Richtmyer viscous pressures used in finite difference methods, [15],

$$\Pi_{ij} = -\zeta_1\frac{(c_i + c_j)(h_i + h_j)}{2(\rho_i + \rho_j)}\psi_{ij} + \zeta_2\frac{(h_i + h_j)^2}{2(\rho_i + \rho_j)}\psi_{ij}^2, \tag{16}$$

$$\psi_{ij} = \begin{cases} \frac{(\mathbf{v}_i - \mathbf{v}_j)\cdot(\mathbf{r}_i - \mathbf{r}_j)}{|\mathbf{r}_i - \mathbf{r}_j|^2 + \eta^2}, & (\mathbf{v}_i - \mathbf{v}_j)\cdot(\mathbf{r}_i - \mathbf{r}_j) < 0, \\ 0, & (\mathbf{v}_i - \mathbf{v}_j)\cdot(\mathbf{r}_i - \mathbf{r}_j) \geq 0, \end{cases} \tag{17}$$

where ζ_1 and ζ_2 are constant artificial viscosity parameters. The term Π_{ij} is positive when particles are aproaching each other and null otherwise. The first term in the equation (16) introduces the shear and the bulk viscosity and the second term helps to prevent particle interpenetration.

3.2. Artificial stress

The artificial stress term acts as a repulsive force between particles which is increased when the separation between particles decreases. That is achieved through the scaling function ϕ_{ij} which is defined as a ratio of the smoothing function values for the actual distance between the pair of particles r_{ij} and the initial particle spacing ${}^0r$,

$$\phi_{ij} = \frac{W(r_{ij})}{W({}^0r)}. \tag{18}$$

Within the quasi-incompressible fluid model, the artificial stress value R_i is taken as

$$R_i = \xi \frac{p_i}{\rho_i^2}, \tag{19}$$

when the value of the pressure p_i is negative, and null otherwise, [14]. The value of parameter ξ is set according to the value of the exponent n and the smoothing length. In the following, the value of exponent n is set equal to 4 and ξ is taken equal to 0.3.

Within the elastic solid model, the artificial stress value is considered

$$R_i^{\alpha\beta} \sim -\xi \frac{\sigma_i^{\alpha\beta}}{\rho_i^2}, \tag{20}$$

when the value of the stress $\sigma_i^{\alpha\beta}$ is positive, and null otherwise, refer to [6] for further details.

The resulting value of the artificial stress factor between two particles is assumed

$$R_{ij}^{\alpha\beta} = R_i^{\alpha\beta} + R_j^{\alpha\beta}. \tag{21}$$

3.3. Correction of particle motion

The stability of the entire calculation may be also improved by implementing the particle motion correcting term, [13], which corrects the value of particle velocity according to the averaged velocity of all neighbouring particles

$$\frac{\mathrm{d}\mathbf{r}_i}{\mathrm{d}t} = \mathbf{v}_i + \varepsilon \sum_j 2m_j \frac{\mathbf{v}_j - \mathbf{v}_i}{\rho_i + \rho_j} W_{ij}. \tag{22}$$

A constant parameter ε is from an interval $\langle 0; 1 \rangle$. This term is usually applied in order to prevent an unphysical particle motion during high speed flows and during simulations of problems involving tension.

4. Fluid-Structure Interaction

There are two major SPH approaches to the material interaction representation applied in practice. The first approach might be called "the summation over all particles" where the governing equations are solved for all particles together, while the second approach treats the particles of every material separately and let them interact through a special interaction algorithm (that might be represented by an application of contact forces at the material interface). The latter approach is applied within this study.

4.1. Contact Algorithm

In order to solve the interaction between fluid and solid material, a contact algorithm is implemented so that the fluid dynamics and the elastodynamics are solved separately. In other words, any fluid particle in the vicinity of an elastic body is not involved within the summation terms in the governing equations for solid body and vice versa. The interaction between fluid and solid particles is realised through contact forces. The contact algorithm implemented within this study is based on the algorithm used by Campbell et al. to treat the interaction of elastic bodies, [2].

The contact algorithm is executed for every pair of fluid and solid particles at a distance less than the thickness of the contact interface. The contact thickness might be defined according to the initial particle spacing, particle radius or by the smoothing length (the radius of the smoothing function support). In the following, the contact thickness equal to the smoothing length is applied. When the particles get into contact, it is possible to evaluate the interface penetration

$$r_p = \frac{1}{2}\left(h_i + h_j\right) - r_{ij}, \tag{23}$$

where r_p is the interface penetration, h is the smoothing length and r_{ij} is the distance between particles. The contact force is applied along the vector connecting the particle centers. An ideally plastic contact is considered, i.e. the force magnitude is estimated so that it brings both particles to rest with respect to each other within a single timestep.

$$F_c = K_p \begin{cases} \max(\mathrm{F}_1, \mathrm{F}_2), & \dot{r}_p > 0, \\ 0, & \dot{r}_p < 0, \end{cases} \tag{24}$$

where

$$F_1 = \frac{(m_i + m_j) r_p}{2\Delta t^2}, \tag{25}$$

$$F_2 = \frac{(m_i + m_j) c_p r_p}{r_{ij} \Delta t}, \tag{26}$$

where F_c is the contact force, Δt is the timestep, c_p is the sound speed and K_p is the scaling parameter. As the numerical value of the sound speed of modelled materials within the simulation presented in section 7 is comparable, the value of c_p is defined as an averaged sound speed of the materials in contact. The contact force F_c is nonzero only for particles which are approaching each other. Above method using the equation (25) is similar to the well-proven penalty contact force algorithm for crashworthiness simulations, [18], where the contact force is applied in normal direction to the contact surface.

5. Rigid Boundaries

The rigid boundaries are represented by two sets of boundary particles, the interface and the wall particles, [19]. When the rigid boundary is fixed, the position of both sets of the boundary particles does not change in time. The interface particles are placed along the boundary surface while the wall particles fill in the region behind the boundary surface to the width of the smoothing function support. Both sets of boundary particles are involved within the summation terms in the governing equations, but only the density and the pressure of the wall particles are evolved. The evolution of boundary particles' density and pressure helps to prevent a penetration of the boundary by active particles (fluid or solid). Despite the fact that the prevention of

boundary penetration may also be enforced by the artificial viscosity (16) and by the correcting term (22), it may eventually happen that some active particles do penetrate the boundary. This may cause a significant corruption of the entire simulation. In order to stabilise the calculation at such cases, an algorithm similar to that of the rigid wall treatment in finite element codes for crashworthiness is applied, [18].

Every interface particle has assigned a normal vector to the boundary surface. When an active particle approaches the boundary interface, an artificial displacement is applied to the active particle along the normal vector of the nearest interface particle. The value of the artificial displacement is set such that the penetration of the boundary is immediately avoided and the new distance between particle and the boundary interface is $r_s = 0.01x_0$, where x_0 is the initial particle spacing. When the artificial displacement is applied, it is necessary to adequately adjust the active particle velocity vector. An artificial velocity $(r_b + r_s)/\mathrm{dt}$ is added to the active particle velocity vector in the direction of the boundary normal, where r_b is the boundary penetration. Even though the artificial displacement causes an additional energy dissipation in the vicinity of the boundary, it is applied to stabilise simulations when penetration of the boundary is imminent.

6. Implementation

An introduction of the relations (1) and (2) enables the evaluation of the function values and their spatial derivatives without a presence of a computational grid. The connectivity of grid-based methods is replaced by the search for the neighbouring particles within the compact support domain of the smoothing function. In this study, the search for the neighbouring particles is realised by the linked-list algorithm, [10]. The time integration of the SPH equations is performed by an explicit numerical integration scheme. Herewith, the predictor-corrector time integrating scheme with appropriate time-stepping conditions is utilised, [6, 16].

7. Numerical simulations

Antoci et al., [1], proposed an experiment involving the interaction of a collapsing column of water with an elastic plate, which they used for validation of their numerical FSI solver. Their experimental setup is designed so that the tests can be analysed as a two-dimensional problem.

The problem of elastic plate subjected to time varying water pressure exerted by a collapsing water column is applied here as a validation of the implemented contact algorithm and the calculated results are compared to experimental as well as computational data published in [1]. The simulation setup is displayed in Fig. 1 (top-left). The fluid particles are coloured in dark grey, the solid particles are black and the rigid boundary is light gray. The column of water is kept between two vertical walls. The lower part of the left wall is elastic while the other parts are considered to be rigid, i.e. the upper part of the left wall, the right vertical wall and the tank bottom are rigid. There is no other obstacle nor wall to the left from the elastic plate so that the water flow can evolve freely in horizontal direction when the elastic plate is released.

The width and the height of the water column are $0.1\,\mathrm{m}$ and $0.14\,\mathrm{m}$, respectively. The elastic plate is $0.005\,\mathrm{m}$ thick and $0.079\,\mathrm{m}$ long. The upper end of the elastic plate is attached to the rigid boundary, while the lower end is released at the beginning of the simulation and is free to move along the rigid bottom. The water density is $1\,000\,\mathrm{kg\,m^{-3}}$ and its dynamic viscosity is $8.9 \times 10^{-4}\,\mathrm{Pa\,s}$. For numerical reasons, the modelled speed of sound in water is $30\,\mathrm{m\,s^{-1}}$ which is lower than its physical value, see section 2.1 The density of the elastic material is

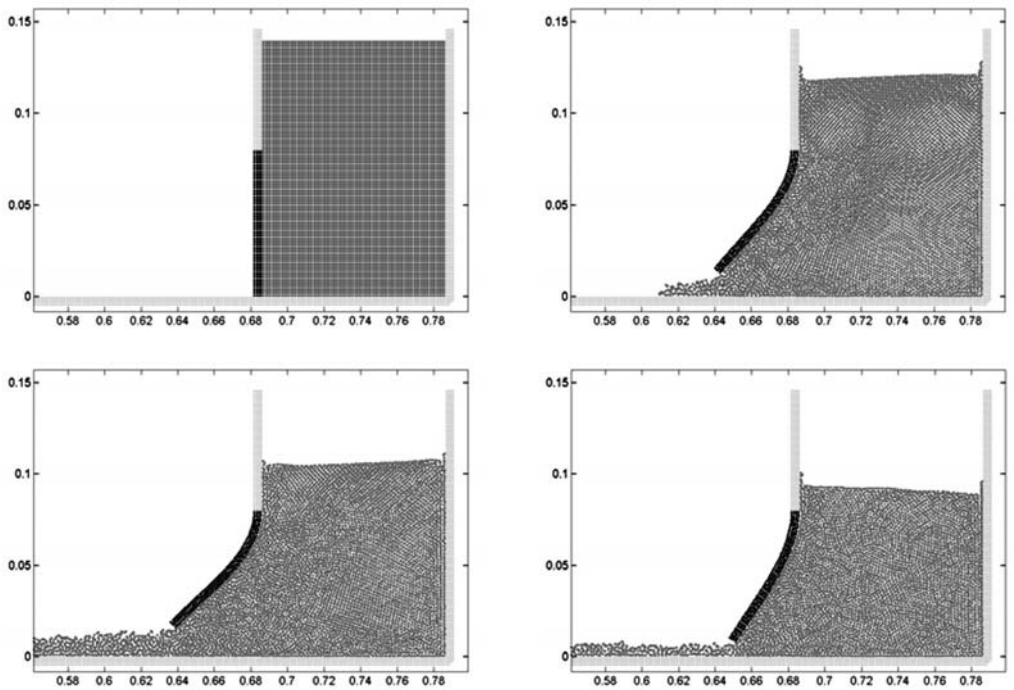

Fig. 1. Elastic plate subjected to time varying water pressure: particle positions at time $0.0\,\mathrm{s}$, $0.09\,\mathrm{s}$, $0.15\,\mathrm{s}$ and $0.33\,\mathrm{s}$

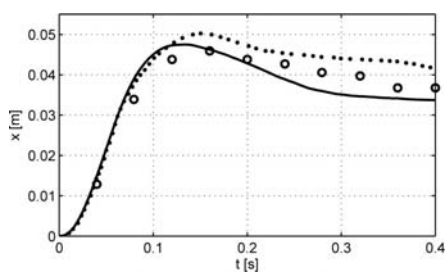

Fig. 2. Free end of the elastic plate: Calculated displacement in x direction (solid line) compared to experimental (circles) and computational (dots) results published by Antoci et al. [1]

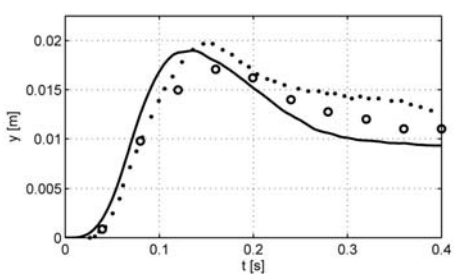

Fig. 3. Free end of the elastic plate: Calculated displacement in y direction (solid line) compared to experimental (circles) and computational (dots) results published by Antoci et al. [1]

$1100\,\mathrm{kg\,m^{-3}}$, its bulk and shear moduli are $2 \times 10^7\,\mathrm{Pa}$ and $4.27 \times 10^6\,\mathrm{Pa}$, respectively. Both artificial viscosity parameters ζ_1 and ζ_2 are equal 1 for the solid material and zero for the fluid. The correction of particle motion parameter ε equals 0.3. The fluid flow is driven by the gravity force while assuming the gravitational acceleration $9.81\,\mathrm{m\,s^{-2}}$.

Fig. 1 shows the evolution of the fluid flow while the elastic plate is deformed under the water pressure. The spatial distribution of SPH particles is displayed at time $0.0\,\mathrm{s}$, $0.09\,\mathrm{s}$, $0.15\,\mathrm{s}$ and $0.33\,\mathrm{s}$, respectively. Naturally, the outflow flux depends on the elastic plate deformation which is evolved by the water pressure. There are apparent free surface waves at the top of the water column which may be observed also in the experiments, [1]. Time evolution of the x and

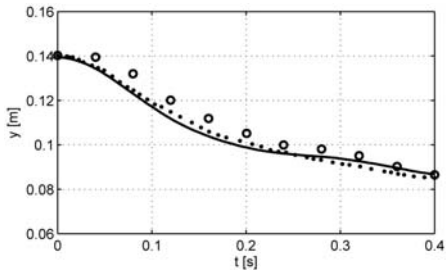

Fig. 4. Water level at the tank center: Calculated water level (solid line) compared to experimental (circles) and computational (dots) results published by Antoci et al. [1]

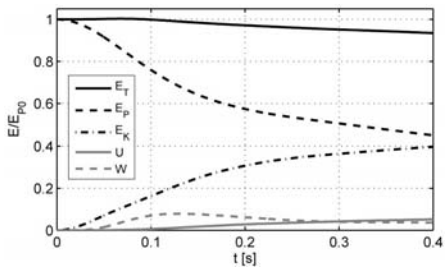

Fig. 5. Energy evolution of the simulated system: E_T total energy, E_P potential energy, E_K kinetic energy, U internal energy of fluid, W deformation energy of solid

y displacement of the elastic plate's free-end is shown in Fig. 2 and 3, respectively. The time evolution and the value of the displacements are in a reasonable agreement with the published data. Even though the maximal displacements of the free-end of the elastic plate are achieved sooner than in the experiments, all trends in the time evolution are well reproduced. In fig. 4, there is a comparison of water level values at the center of the tank. Again a good agreement is achieved. The numerical model is slightly dissipative, due to the introduction of corrective terms and due to the applied rigid boundary model. There is an apparent drop of the total energy of the simulated system displayed in fig. 5, which is about 6.5 %.

The key issue of the performed simulations is a proper choice of the contact force scaling factor K_p. In case its value is set too large, a void area along the contact interface may appear, on the other hand when its value is too small, there is a danger of an inter-penetration of the materials in contact. The value $0.002\,5$ for the scaling factor K_p is applied in the presented simulation. When a definition of the contact thickness is modified to the value of initial particle spacing and the scaling factor value is 0.25, nearly identical results are obtained.

8. Conclusion

The presented results of the SPH simulations give a satisfactory agreement with the results of experiments and numerical simulations performed by Antoci et al., [1]. The applied contact algorithm for solution of the FSI problem by introducing a contact (penalty) force acting along the centerline of the interacting particles is very simple and straightforward to implement. Even though this is a simple approach to interaction modelling, the algorithm is very flexible, stable and relatively modest in terms of computational costs. It may be advantegeous for simulations of problems involving fractures and other changes in the interface topology as no contact surface has to be defined.

Despite the satisfactory results presented, a study of the sensitivity of the contact algorithm to the parameter setup and an identification of an optimal choice for the scaling factor K_p value for a general paramater setup are of interest. Eventually, a modification of the presented algorithm so that the contact force is applied in the boundary normal direction can be considered.

Acknowledgements

This work is supported by the research project MSM 4977751303 of the Ministry of Education, Youth and Sports of the Czech Republic.

References

[1] C. Antoci, M. Gallati, S. Sibilla, Numerical simulation of fluid-structure interaction by SPH, Computers and Structures 85 (2007) 879–890.

[2] J. Campbell, R. Vignjevic, L. Libersky, A contact algorithm for smoothed particle hydrodynamics, Computer Methods in Applied Mechanics and Engineering 184 (2000) 49–65.

[3] A. Colagrossi, M. Landrini, Numerical simulation of interfacial flows by smoothed particle hydrodynamics, Journal of Computational Physics 191 (2003) 448–475.

[4] S. Comas-Cardona, P. H. L. Groenenboom, C. Binetruy, P. Krawczak, A generic mixed FE-SPH method to address hydro-mechanical coupling in liquid composite moulding processes, Composites: Part A 36 (2005) 1 004—1 010.

[5] R. A. Gingold, J. J. Monaghan, Smoothed Particle Hydrodynamics: theory and application to non-spherical stars, Monthly Notices of the Royal Astronomical Society 181 (1977) 375–389.

[6] J. P. Gray, J. J. Monaghan, R. P. Swift, SPH elastic dynamics, Computer Methods in Applied Mechanics and Engineering 190 (2001) 6 641–6 662.

[7] P. H. L. Groenenboom, B. K. Cartwright, Interaction between structures and waves using the coupled FE-SPH method, in Proc. of the International Conference on Computational Methods in Marine Engineering MARINE 2007, CIMNE, Barcelona, 2007.

[8] P. H. L. Groenenboom, High-velocity impact simulation by a hybrid SPH-FE method in PAM-SHOCK, in Proc. of the 2nd SPHERIC International Workshop, ETSIN UPM, Madrid, 2007, pp. 13–14.

[9] L. D. Libersky, A. G. Petschek, Smooth Particle Hydrodynamics With Strength of Materials, in Advances in the Free-Lagrange Method Including Contributions on Adaptive Gridding and the Smooth Particle Hydrodynamics Method, Lecture Notes in Physics, Springer, 1991, pp. 248–257.

[10] G. R. Liu, M. B. Liu, Smoothed Particle Hydrodynamics, World Scientific Publishing, Singapore, 2003.

[11] L. Lucy, A numerical approach to the testing of the fission hypothesis, Astronomical Journal 82 (1977) 1 013–1 020.

[12] J. J. Monaghan, Smoothed Particle Hydrodynamics, Annual Review of Astronomy and Astrophysics 30 (1992) 543–574.

[13] J. J. Monaghan, Simulating free surface flows with SPH, Journal of Computational Physics 110 (1994) 399–406.

[14] J. J. Monaghan, SPH without a tensile instability, Journal of Computational Physics 159 (2000) 290–311.

[15] J. J. Monaghan, R. A. Gingold, Shock simulation by the particle method SPH, Journal of Computational Physics 52 (1983) 374–389.

[16] J. P. Morris, P. J. Fox, Y. Zhu, Modeling low Reynolds number incompressible flows using SPH, Journal of Computational Physics 136 (1997) 214–226.

[17] G. Oger, M. Doring, B. Alessandrini, P. Ferrant, Two-dimensional SPH simulations of wedge water entries, Journal of Computational Physics 213 (2006) 803–822.

[18] PAM-CRASH Theory Notes Manual, ESI-Group Trademark, 2000.

[19] D. Violeau, R. Issa, Numerical modelling of complex turbulent free-surface flows with the SPH method: an overview, International Journal for Numerical Methods in Fluids 53 (2007) 277–304.

[20] R. Vignjevic, Review of development of the Smooth Particle Hydrodynamics (SPH) method, in Proc. of 6th Conference on Dynamics and Control of Systems and Structures in Space, Cranfield University, 2004, pp. 23–44.

[21] T. De Vuyst, R. Vignjevic, J. C. Campbell, J.C., Coupling between meshless and finite element methods, International Journal of Impact Engineering 31 (2005) 1 054–1 064.